Kovove Mater. 62 2024 313–325
DOI: 10.31577/km.2024.5.313

Improvement and characterization of the surface properties of AA 5083 aluminum alloy by plasma spraying methods

Mehmet Temel[1], Ilhan Celik[2]*, Bayram Benli[1]

[1]*Department of Mechanical Engineering, Institute of Graduate Programs, Samsun University, Samsun, Turkye*
[2]*Department of Mechanical Engineering, Faculty of Engineering and Natural Sciences, Samsun University, Samsun, Turkye*

Received 30 August 2024, received in revised form 4 October 2024, accepted 31 October 2024

Abstract

In this study, plasma spraying methods with 100 % Al_2O_3 (AT0), 87 % Al_2O_3 + 13 % TiO_2 (AT13), and 60 % Al_2O_3 + 40 % TiO_2 (AT40) coatings were applied to the surface of aluminum alloy (AA 5083). After the coating processes, the structural analyses of the samples were performed using an XRD device. The thicknesses of the obtained coatings were measured with a DURAMIN-40 M1 MSO-04 device. The surface hardness values of the samples were determined using a microhardness testing device with parameters of 100 g load and 15 seconds duration. Scratch tests to determine the adhesion of the coatings to the substrate were conducted using a UMT-2MT testing device. Additionally, the surface roughness values of the samples were measured with a PCE-RTE 2000 device. The wear behavior of the samples after the coating processes was examined using the UMT-2MT testing device. The surface morphologies of the samples and the surfaces after wear tests were analyzed in detail using an SEM device. According to the research results, the highest coating thickness was obtained in AT13-coated samples (512 μm), while the lowest coating thickness was measured in anodized samples (47 μm). In the scratch tests, the best performance was observed in AT13-coated samples (52 N), while the lowest performance was determined in AT13-coated samples (36 N). It was observed that all coating processes resulted in an improvement in wear resistance.

Key words: wear, scratch test, SEM, XRD

1. Introduction

Materials hold an indispensable place in every aspect of our daily lives. Each material has its unique characteristics; properties such as density, corrosion resistance, electrical conductivity, heat resistance, and strength vary from one element to another. Therefore, selecting a material that meets the specific requirements of its intended application is of great importance. However, in material selection, technical properties and factors like cost, durability under usage conditions, corrosion, and wear resistance must be considered. The high cost of materials like gold, silver, or titanium often leads to the preference for alternative, low-cost materials that are more readily available in the market, as the cost factor is important.

The physical and chemical processes applied to the entire material are also among the factors that increase costs. Therefore, the development of surface treatment/coating technologies becomes increasingly important. The primary goal of surface treatments is to enhance the quality and performance of the material used while reducing overall costs [1]. This technology is implemented by coating the material's surface with a different material or by forming an oxide layer rather than processing the entire material. In this way, the surface's corrosion resistance, wear behavior, and friction properties are improved without compromising the material's overall characteristics [2]. Additionally, more aesthetically pleasing and robust products can be produced by enhancing the material's lifespan, fatigue resistance, and wear durability. Therefore, the research and development of surface technologies hold significant importance world-

---

*Corresponding author: e-mail addresses: ilh.celik@gmail.com, ilhan.celik@samsun.edu.tr

Table 1. Chemical composition of AA 5083 alloy (wt.%)

Alloy	Cu	Mg	Mn	Fe	Zn	Ti	Cr	Si	Al
AA5083	0.1	4.0–4.9	0.4–1.0	0.4	0.25	0.15	0.05–0.25	0.4	The rest

wide [3–5]. In most cases, wear resistance is one of the most critical criteria in selecting machine parts and tool materials during the design process and operational conditions. One method used to enhance wear resistance is the plasma spraying technique. The most commonly employed coatings in this method are aluminum oxide-based ceramic coatings, often combined with titanium oxide. To increase the wear resistance and extend the lifespan of composite molds, the tips of these molds were coated with a 60 % Al_2O_3-40 % TiO_2 ceramic coating using an atmospheric plasma spray method and an interlayer. The high-chromium mold tips, which contain elements such as C, Si, Mn, P, S, Cr, Mo, Ni, Cu, B, and Fe, were subjected to an abrasive process using an air jet-fed abrasive material before the ceramic coating. This process aimed to enhance surface development and improve the adhesion of the interlayer (NiAlCrSi) to the surface. Subsequently, the surface was coated with a ceramic material prepared at a 60 % Al_2O_3-40 % TiO_2 ratio using the atmospheric plasma spraying method. The wear test results showed that in the case of ceramic coating, the penetration depth of the diamond cutting tip was almost half the penetration depth when scratching the surface of high chromium cast iron. The application of the interlayer combined with ceramic coating significantly contributed to the formation of much higher resistance to abrasive materials [6].

Pure aluminum is a soft, corrosion-resistant, and lightweight metal. Its density at 20 ℃ is 2.7 g cm^{-3} [7]. It has a high strength-to-density ratio and is corrosion-resistant [8]. Its machinability, ability to form alloys with many metals, cost-effectiveness, availability of raw materials, and advanced production techniques make it one of the preferred metals in material selection [3, 9, 10]. The lightness and corrosion resistance of aluminum make it play a significant role in aerospace and space technology [11]. Due to its casting ability, it can be used in engine blocks, and due to its low density and lightness, it can be used in marine and watercraft applications [12, 13]. Its structure is suitable for anodic coating, which makes it preferred in medical applications and the production of various decorative products. The lightness of aluminum, its high material quality, and abundance on Earth make it stand out [9]. Aluminum can form different alloys by alloying with elements such as silicon, iron, manganese, magnesium, and nickel in various percentages. These alloys are classified based on whether they have undergone heat treatment or tempering (annealing). The AA 5083 alloy used in this study belongs to the 5000 series. This alloy is widely used in marine environments and the defense industry [14].

Every material on Earth will eventually reach the end of its lifespan. Since the physical and chemical properties of materials do not always provide sufficient protection against effects such as corrosion, wear, and friction, technological efforts are made to improve these properties. In this study, different coating types were applied to enhance the surface properties of the commonly used AA 5083 aluminum alloy. Plasma spraying processes were applied to the samples, and microhardness, wear, scratch tests, surface roughness, surface morphology, XRD, SEM, and 3D profilometer analyses were conducted. The main objective of the study is to significantly improve the tribological properties of the surface compared to the uncoated material. In this context, plasma spraying techniques were thoroughly examined, and the obtained data were evaluated.

2. Material and method

2.1. Material

This study used aluminum 5083 alloy samples with dimensions of 20 mm × 20 mm × 4 mm as the base material. The composition ratios of the alloy are shown in Table 1.

The surfaces of the aluminum 5083 alloys were meticulously sanded using SiC wet sandpapers, starting with 60 mesh and progressing through 400, 800, 1200, 2000, and 3000 mesh. The sanded surfaces were then thoroughly cleaned with ethanol and dried using a drying device to ensure no stains remained. After these processes, the samples were prepared for coating. Figure 1 shows images of the sanded base material and the coated samples.

2.2. Coating powders

For the 100 % Al_2O_3 (AT0) coating process of the AA5083 alloy surface, Oerlikon Metco Amdry 956 binding powder and Amdry 6060 Al_2O_3 coating powder were used. Alumina, one of the most commonly used materials among engineering ceramics, is chemically inert and stable at high temperatures. This hard and wear-resistant material exhibits excellent electrical insulation (dielectric properties) and thermal con-

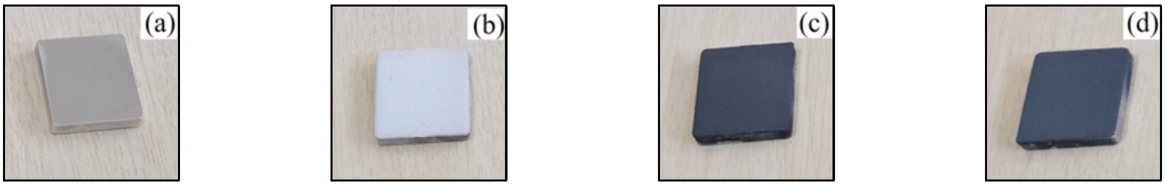

Fig. 1. Test materials (AA 5083): (a) uncoated, (b) AT0 coated, (c) AT13 coated, and (d) AT40 coated.

Table 2. Parameters used in coating processes

Coating Parameters	AT0	AT13	AT40
Current (A)	500	500	500
Voltage (V)	65–70	70–80	65–70
Carrier gas flow, Ar ($\mathrm{l\,min^{-1}}$)	38	16	16
Secondary gas, H_2 ($\mathrm{l\,min^{-1}}$)	7	20	15
Plasma gas, Ar ($\mathrm{l\,min^{-1}}$)	80	80	100
Spray distance (mm)	50–100	100–125	150
Gun speed ($\mathrm{mm\,s^{-1}}$)	5–6.7	5–6.7	5–6.7
Table rotation speed ($\mathrm{cm\,s^{-1}}$)	125	125	125
Powder feed amount ($\mathrm{g\,min^{-1}}$)	42	38	23

ductivity with high purity grades (i.e., white alumina). These characteristics, along with its low cost, make alumina suitable for a wide range of engineering applications. The material + TiO_2 (87 %-13 %) (AT13) coating process, Oerlikon Metco Amdry 956 binding powder and Amdry 6228 Al_2O_3 + TiO_2 coating powder were used. Powders containing alumina and 13 % titanium oxide (nominal) are designed to produce dense, wear-resistant ceramic coatings that can be ground to achieve excellent surfaces. For the Al_2O_3 + TiO_2 (60 %-40 %) (AT40) coating process, Oerlikon Metco Amdry 956 binding powder and Amdry 6257 Al_2O_3 + TiO_2 coating powder were used. Powders containing alumina and 40 % titanium oxide are suitable for applications requiring moderate hardness and grindability but higher fracture toughness than pure alumina or alumina coatings with 3 or 13 % titanium oxide. These coatings provide hard and durable surfaces at operating temperatures up to 540 ℃. They are recommended for applications requiring resistance to abrasive particles, wear, and particle erosion. Due to their low wettability when polished, they are ideal for applications resistant to mildly acidic environments in the chemical processing industry.

2.3. Coating parameters

The atmospheric plasma spraying method was used for the coating processes. For coating the AA 5083 alloy, binding powder, coating powder, and a spray gun were employed. The binding powder and coating powder were applied to the sample surface using the spray gun according to specific parameters. The fundamental parameters used during production, such as current, voltage, and gun distance, are detailed in Table 2.

2.4. Structural and mechanical analysis

Structural analyses of samples subjected to different coating processes were performed using a Rigaku Smart Lab X-ray Diffractometer with a CuKα radiation source. The measurements were conducted with a wavelength of $\lambda = 1.5405$ Å and a scanning angle of $2\theta = 20°$–$80°$ at a rate of $2°\ \mathrm{min^{-1}}$ in a symmetric scanning configuration. The AA 5083 alloy samples with coatings were first subjected to a mounting process. They were sanded and polished to obtain cross-sectional images of the mounted samples. Subsequently, the thickness measurements of the samples were carried out with the assistance of a Duramin-40 M1 MSO-04 device. Figure 2 shows images of the mounted samples.

The microhardness values of the samples were measured using a Duramin-40 M1 MSO-04 microhardness measurement device. The tests were conducted using a Vickers indenter under a load of 100 grams for 15 seconds, and at least three measurements were taken. Scratch tests on the coated samples were performed using a Universal Tribometer mod. UMT-2MT testing block s/n T45881 device with a Rockwell-C diamond tip. The scratch tests were conducted with a force increasing from zero to 100 N over a distance of 10 mm at a speed of $0.16\ \mathrm{mm\,s^{-1}}$ for 3 minutes and 30 seconds. Surface roughness measurements were carried out using a PCE-RTE 2000 device. Measurements were taken at least three points on the surfaces of the samples according to the Gauss 3 × 0.80 param-

Fig. 2. Image of the samples embedded in bakelite.

Table 3. Parameters of the wear tests

Test parameters	Values
Test type	Reciprocating
Applied load (N)	10
Wear distance (mm)	10
Speed (mm s^{-1})	10
Test time (s)	5100
Counter ball material	WC
Temperature (℃)	Room temperature (23 ± 2)
Environment	Dry conditions

eters, and the roughness value was calculated by averaging the obtained values. Wear tests of untreated and coated samples with different coating types were performed using a Universal Tribometer mod. UMT-2MT testing block s/n T45881 wear testing device. The wear distance in the wear tests was 51 meters. The wear track profiles were recorded using a 3D profilometer to calculate the wear volume loss, and the wear rates were calculated using the Archard equation. The wear tests were conducted using the test parameters provided in Table 3.

To visualize the wear traces of the samples subjected to wear tests in three dimensions, a CNT-01 3D optical profilometer was used. This allowed for determining the wear rates resulting from the wear tests. The SEM and EDS analyses of the samples were conducted using a JOEL JSM-7001F scanning electron microscope.

3. Results and discussion

3.1. XRD analysis

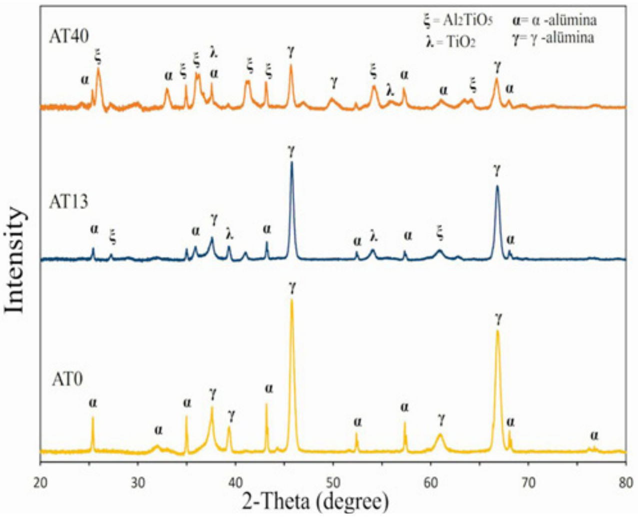

Fig. 3. XRD graphs of AT0, AT13, and AT40 samples.

Figure 3 presents the XRD results for the AT0, AT13, and AT40 samples. The XRD analysis of the AT0 sample shows that the coating structure includes α-alumina and γ-alumina phases. The highest peak positions are at $2\theta = 46°$ and $2\theta = 67°$, with these peaks identified as belonging to γ-alumina. The obtained peaks were determined to be consistent with the literature [15–17]. While the AT0 sample contains thermodynamically stable 100 % α-Al_2O_3 particles, it was found that the obtained coating consists of both γ-Al_2O_3 and α-Al_2O_3 phases. Due to the high cooling rate of molten alumina droplets during plasma spraying and the lower interfacial energy between the liquid and the crystal, γ-Al_2O_3 is thought to nucleate more easily compared to α-Al_2O_3 during cooling and solidification. This results in a more pronounced formation of γ-Al_2O_3 in the coating structure [15–18]. The alpha (α) phase is associated with unmelted or partially melted alumina powder particles or with melted powder particles that cool at a lower rate. The nucleation of the metastable gamma (γ) phase and the formation of the amorphous phase are related to the rapid cooling of molten splats on the substrate metal surface [19, 20].

Upon examining the XRD results of the AT13 samples, it is observed that the highest peak positions at $2\theta = 46°$ and $2\theta = 67°$ are attributed to γ-alumina [15, 21–25]. For the AT40 sample, the highest peak is observed at $2\theta = 27°$, and this peak is identified as being composed of the Al_2TiO_5 phase [15, 21, 22, 26–28]. When the XRD patterns of the AT13 and AT40 samples are evaluated together (Fig. 3), it is observed that the coatings generally consist of Al_2O_3, TiO_2, and Al_2TiO_5 phases. Additionally, XRD analyses from other studies in the literature show similar phase compositions [15, 21, 23–25, 28, 29]. The coatings exhibit the broadest peaks for Al_2O_3. Some of the Al_2O_3 phases are α-Al_2O_3, while others are γ-Al_2O_3. The coating powders primarily consist of α-Al_2O_3 phases before the coating process. During the plasma spraying process, a portion of the α-Al_2O_3 phase transforms into γ-Al_2O_3 [21, 22, 30]. The presence of TiO_2 in the structure of these types of coatings contributes to a lower porosity in Al_2O_3 coatings, making them less brittle and enhancing their wear resistance [23]. In atmospheric plasma sprayed coatings with increasing TiO_2 content, the proportion of α-Al_2O_3 phase in Al_2O_3-$40TiO_2$ coatings has been reported to increase from 10 to 17 % [31]. Alumina and alumina-titania systems can exhibit various phase and crystallographic structure changes depending on the cooling process, deposition techniques, material spraying conditions, the ratio of each component, and the properties of the used binder layer [26, 32].

3.2. Film thickness measurements and cross-sectional images of the coatings

Cross-sectional images of the coatings obtained on the surface of AA5083 alloy using the plasma spraying method are presented in Fig. 4. Bond coatings are widely preferred in many industrial plasma spray applications and serve crucial functions. Since the substrate and the main coating often have different thermal expansion coefficients, a bond coating layer must ensure a compatible thermal expansion match between these two layers. Although bond coatings are always thinner than the main coatings, this thin layer plays a critical role in enhancing the overall performance and durability of the coating system [33, 34]. The coatings with different compositions applied to the surface of AA5083 alloy exhibit significant differences. Firstly, a coating with a thickness of 123 μm was achieved with 100 % Al_2O_3 (AT0). This coating provided the surface with a homogeneous ceramic structure. Secondly, the coating with a composition of 87 % Al_2O_3 + 13 % TiO_2 (AT13) reached a remarkably high thickness of 512 μm. Lastly, the coating containing 60 % Al_2O_3 + 40 % TiO_2 (AT40) had a thickness of 211 μm and exhibited a more balanced coating structure with the change in composition.

3.3. Surface morphology

Figure 5 shows the SEM images of the coated surfaces for the AT0, AT13, and AT40 samples. The SEM images reveal that the AT0 coating surface has a wavy structure, with aluminum particles creating pores in the coating layers, some localized defects, unmelted or partially melted particles, powder agglomeration, and cracks forming towards the substrate beneath the lamellae. For the AT13 and AT40 samples, the SEM images indicate the presence of micro-cracks, areas of incomplete contact between lamellae, pores in the coating layers, and the formation of an oxide layer on the surface (Figa. 5b,c). Additionally, melted or partially melted particles are present on the coating surface, creating a wavy appearance. It is noted that porosity varies with the wt.% TiO_2 content, increasing with higher TiO_2 amounts. In Al_2O_3-TiO_2-based coatings applied to AISI 304 stainless steel surfaces using plasma spraying, it has been reported that porosity decreases with increasing TiO_2 content, which is

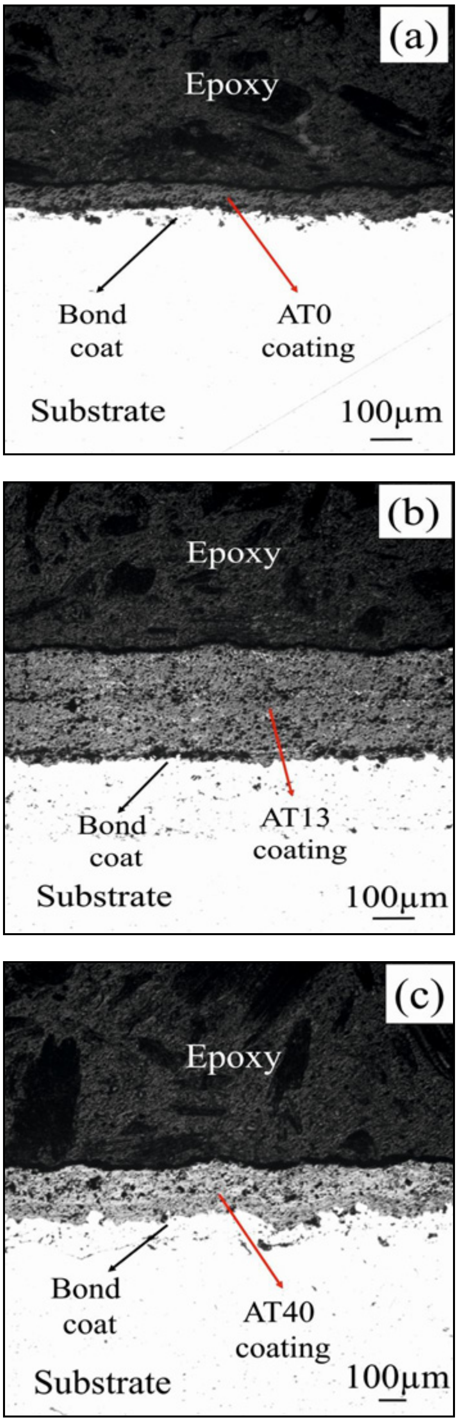

Fig. 4. Cross-section micrographs of the specimens: (a) AT0, (b) AT13, and (c) AT40.

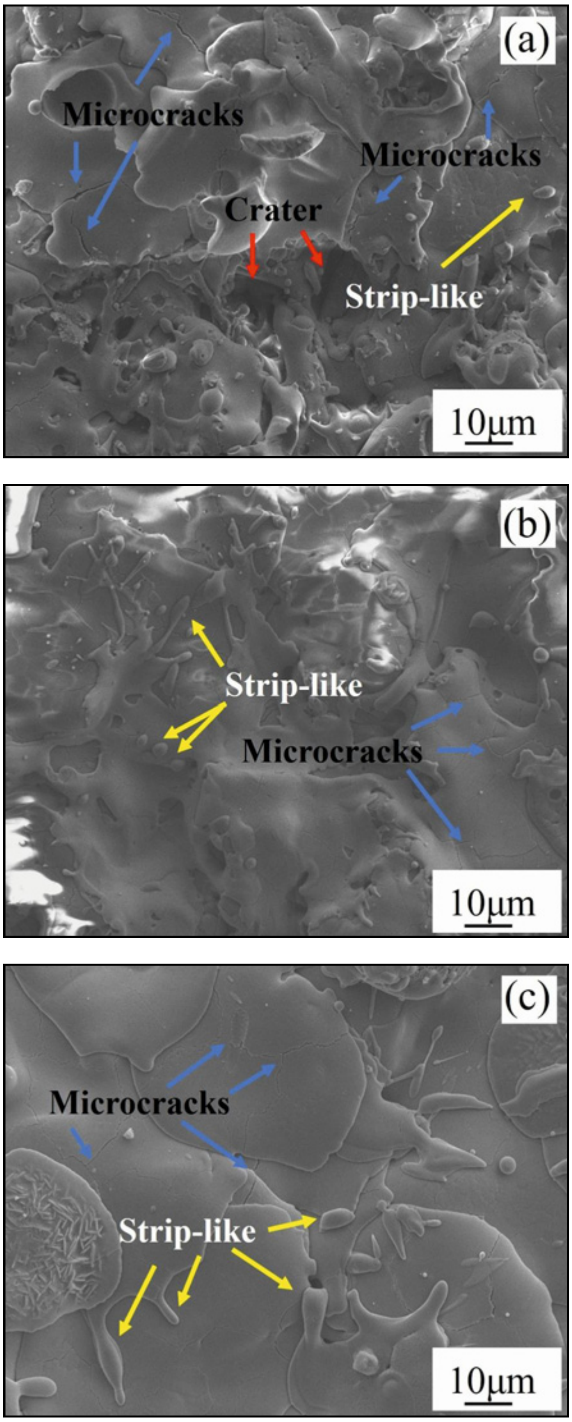

Fig. 5. The surface images of coated AA5083 specimens: (a) AT0, (b) AT13, and (c) AT40.

related to the approach of the mixture's composition to the eutectic composition in the Al_2O_3-TiO_2 binary phase diagram as TiO_2 content increases [35].

3.4. Scratch test analysis

The scratch test results for the AT0 sample are detailed in Fig. 6a. In this test, the critical load value determined for assessing the coating's durability, Lc, was found to be $Fz = 52$ N. This result indicates that the coating has high scratch resistance. The scratch test results for the AT13 sample are presented in Fig. 6b. For this sample, the coating's durability was evaluated with a critical load value, Lc, of $Fz = 36$ N. This lower value suggests that the AT13 coating has lower scratch resistance than the AT0. The scratch test results for the AT40 sample are shown in Fig. 6c. The critical load value Lc was determined to be $Fz = 44$ N, indicating higher durability than AT13 but lower than AT0.

3.5. Micro-hardness analysis

The microhardness test analysis results for the untreated and differently coated AA 5083 samples are presented in Table 4. The data in the table show the microhardness differences between the samples. For a clearer understanding of these differences, the comparative microhardness averages of the relevant samples are graphed in Fig. 7.

When comparing the measured hardness values for AA 5083 alloy between untreated and coated conditions, it has been determined that the coatings increase the microhardness values. The AT0 coating exhibits the highest hardness value for AA 5083 alloy, followed by the AT13 and AT40 coatings in that order. It has been observed that the hardness decreases with an increasing TiO_2 ratio in Al_2O_3 coatings [36]. The microhardness values of the AT0 and AT13 coatings are quite high. Similar studies have shown that these coatings exhibit similar behavior in terms of microhardness values [15, 21, 22, 33].

3.6. Wear test analysis

Figure 8a shows that the coefficient of friction measured for the uncoated sample is 0.539 ± 0.074. Figure 8c presents SEM images of the uncoated AA 5083 alloy after the wear test, while Fig. 8b shows the 3-dimensional profilometer images. It was found that wear led to surface fractures and plastic deformation.

The wear behavior of ceramic coatings is influenced by factors such as hardness, fracture toughness, surface roughness, microstructure, porosity, micro-cracks, and inter-lamellar boundaries. Significant differences in abrasive wear rates and coefficient of friction of aluminum have been observed. The coefficient of friction shows an increasing trend during the initial run-in period and then in the steady-state regime. Since the contact between abrasive particles and the surface occurs at only a few rough contact points, the initial increase is due to the local increase in contact stress. With further sliding, the real contact area increases due to deformation at the rough contact points, lead-

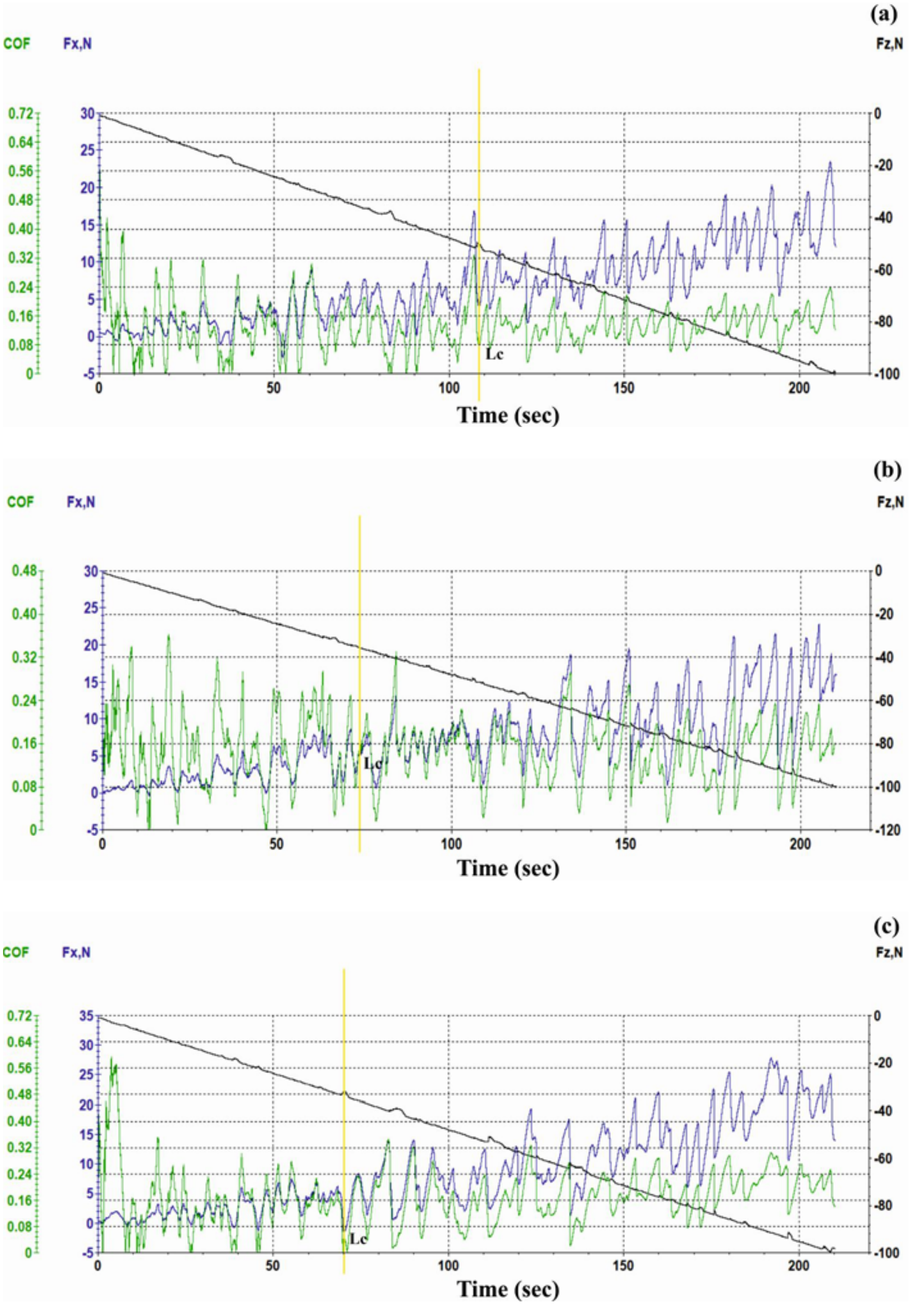

Fig. 6. Scratch test plots of the coated specimens: (a) AT0, (b) AT13, and (c) AT40.

Table 4. Microhardness, friction coefficient, and wear rate values of the samples

Specimens	Microhardness ($HV_{0.1}$)	Friction coefficient (μ)	Wear rate ($mm^3\ N^{-1}m^{-1}$)
Uncoated	87 ± 2	0.539 ± 0.074	1.72×10^{-4}
AT0	1426 ± 57	0.501 ± 0.049	1.46×10^{-5}
AT13	1379 ± 55	0.504 ± 0.063	1.69×10^{-5}
AT40	826 ± 32	0.562 ± 0.021	2.24×10^{-5}

ing to a reduction in contact stress [37]. For example, in the graph curve shown in Fig. 9a, it can be observed that the initial coefficient of friction value starts to increase after the first contact point, and then remains constant at a steady friction coefficient once the contact area with the surface reaches a certain level. This

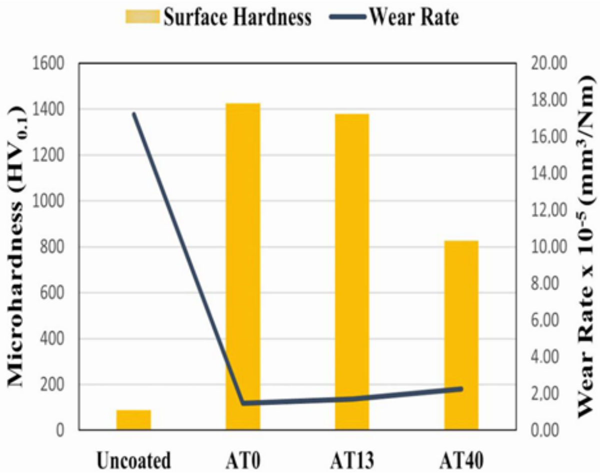

Fig. 7. Microhardness values and wear rates of the samples.

behavior is thought to be due to the increase in contact area and the balancing of the frictional forces.

Comparing the coefficient of friction versus time graphs in Figs. 8a, 9a, 10a, and 11a, it has been determined that the friction coefficients for the AT0 and AT13 samples are lower than those of the uncoated AA 5083 samples. In contrast, the friction coefficient of the AT40 sample is higher than that of the untreated sample. These results clearly demonstrate the effect of different coating types on the frictional behavior of AA 5083 alloy. It has been found that as the TiO_2 content in AT0, AT13, and AT40 increases, the coefficient of friction also rises. Examination of the friction coefficients of the coated samples reveals that the average friction coefficient is highest for the AT40 sample (Table 4), followed by AT13 and AT0. The similarity in microhardness values between the AT13 and AT0 samples results in similar levels of wear resistance. Literature studies indicate that as the TiO_2 content in alumina-based coatings increases, the hardness of the material decreases, leading to a corresponding increase in wear rate [22, 38].

Hardness has a significant impact on wear resistance. The higher the hardness, the better the wear resistance. Increasing microhardness leads to improvements in the wear resistance of coatings. Additionally, grain size also affects wear resistance. A reduction in grain size enhances wear resistance, thereby improving the performance of the coating. These findings underscore the importance of considering both hardness and grain size in the design of coating materials [39]. When comparing microhardness with wear rates, it was found that the highest microhardness value occurred in the AT0 sample, and the least wear also occurred in the AT0 sample. These results indicate that there is an inverse relationship between microhardness and wear rate, with the least wear occurring in the AT0 sample. Ceramic coatings exhibit a high degree of elastic recovery during load release and contribute to low plastic deformation during contact with the indenter. The substantial elastic recovery of the coatings is beneficial in reducing damage caused by impact and abrasive wear. These properties enhance the durability and service life of ceramic coatings, allowing the material to remain resistant to wear and impacts for a longer period [40]. Wear is a critical process in terms of material performance and durability. An increase in

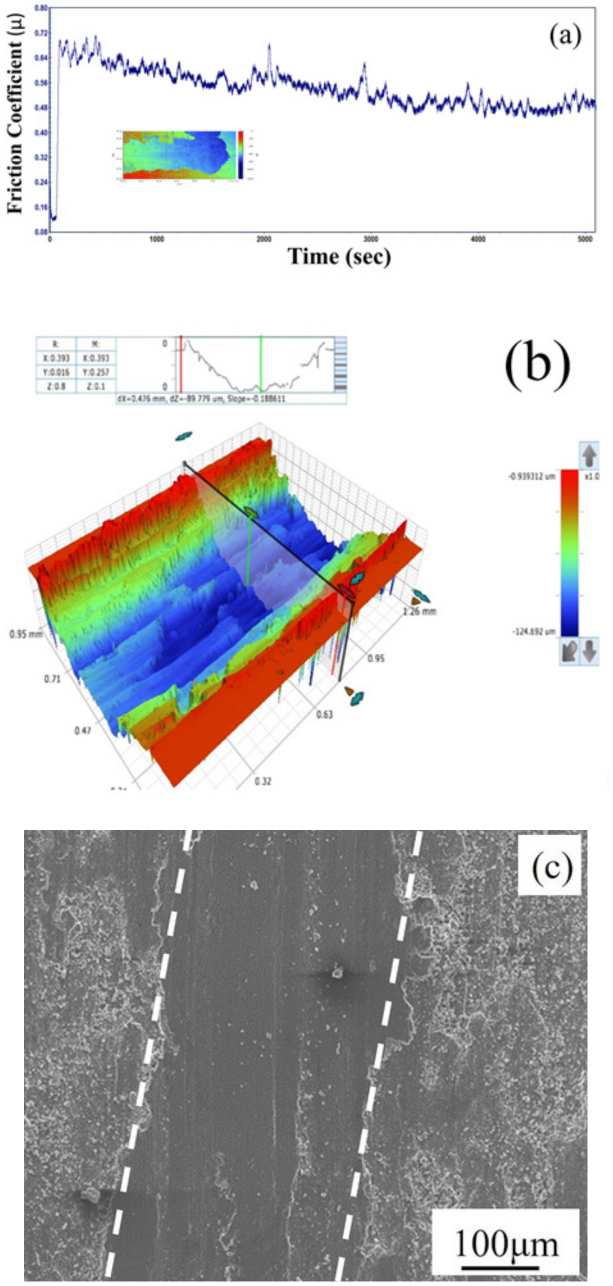

Fig. 8. Wear test results of uncoated sample: (a) friction coefficient-time graph, (b) 3D profilometer image of wear scar, and (c) SEM image of wear scar.

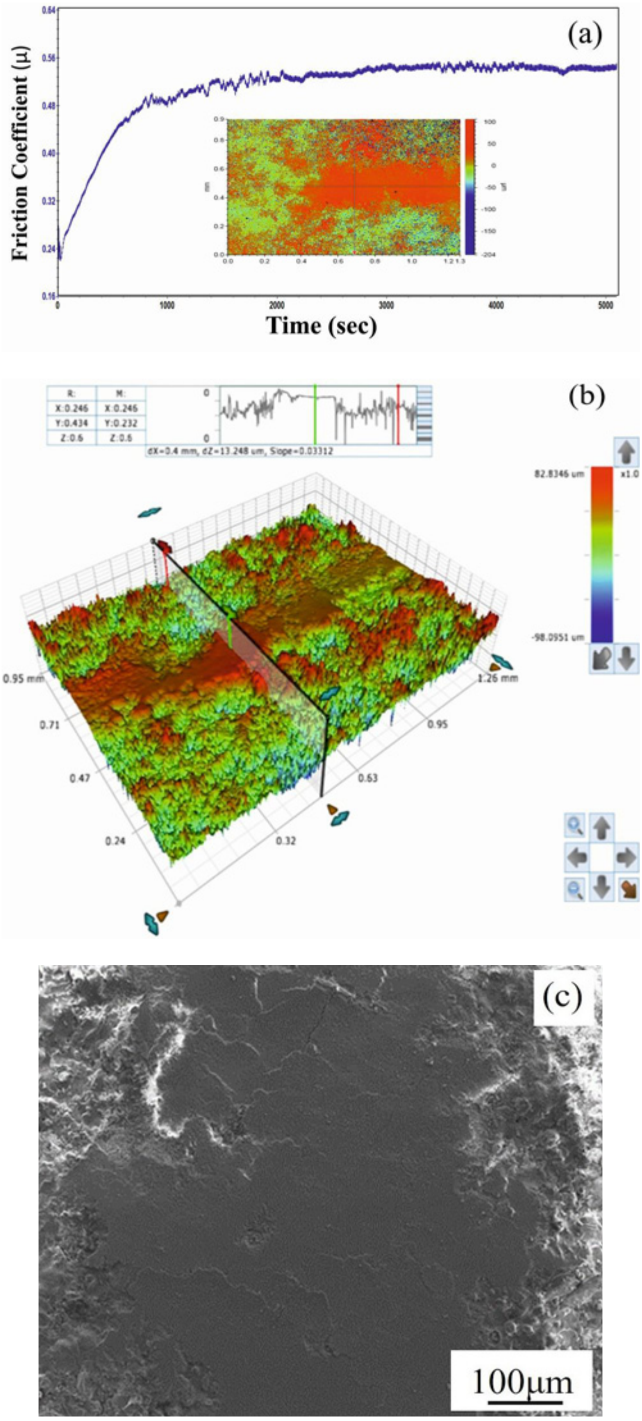

Fig. 9. Wear test results of AT0: (a) friction coefficient-time graph, (b) 3D profilometer image of wear scar, and (c) SEM image of wear scar.

wear amount can lead to the detachment of particles from the surface, which can cause abrasive wear. This process results in the deterioration of surface properties and a reduction in overall structural integrity. Controlling the amount of wear is crucial for extending the lifespan of the material and maintaining its func-

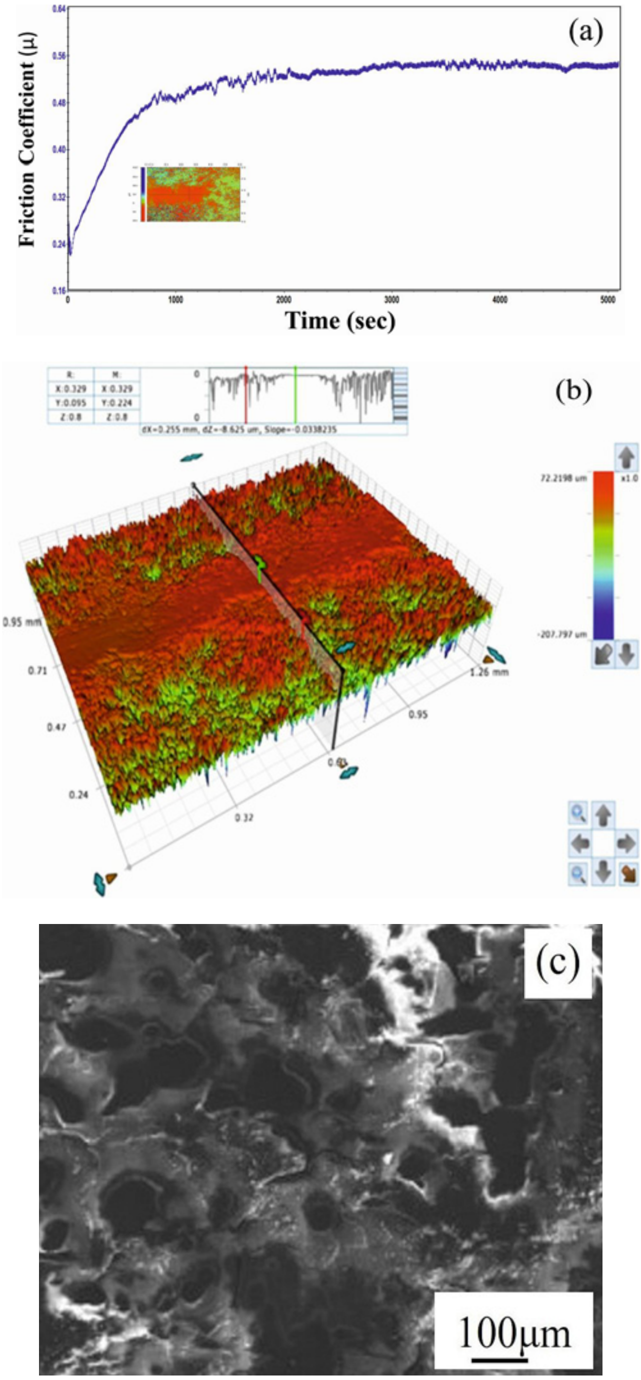

Fig. 10. Wear test results of AT13: (a) friction coefficient-time graph, (b) 3D profilometer image of wear scar, and (c) SEM image of wear scar.

tionality. According to the data in Table 4, the highest wear rate is observed in the uncoated AA 5083 sample, while the lowest wear rate is seen in the AT0 sample. The wear rates for AT13 and AT40 coated samples follow these values, respectively.

It has been observed that the coatings applied to the samples reduced the wear rate compared to the uncoated samples, and the coating processes generally increased the wear resistance. In coatings produced by plasma spraying, an increase in the wt.% of TiO_2 was observed to result in an increase in wear amount. During the coating process of AA5083 aluminum samples, it was observed that the flame from the gun created high-temperature smoke, and the particles within this smoke melted. These molten droplets formed a micro-level laminar and dense coating upon striking the substrate at high speeds. Due to the high speed of the flame and the distance between the gun and the substrate, it was observed that some powder particles did not fully melt during the process, creating partially molten areas on the substrate [12]. Examinations conducted on the coated samples show that the coating material particles created a rough surface area where they adhered [3]. The microstructure of the coating has been found to be largely dependent on the selected process parameters [41]. The microstructure and characteristics of the obtained coating are influenced not only by the parameters of the feed powder but also by wear test conditions such as load, lubrication environment, and temperature [12].

When examining the SEM image of the worn surface of the AT0 sample shown in Fig. 9c, it is observed that microcracks have formed due to wear, with the presence of unmelted powder particles, and the worn area has a rougher texture compared to the unworn area. Additionally, this is visible in the 3-D profilometer image shown in Fig. 9b. The irregular wear is believed to be caused by voids between the lamellae.

Fig. 10c presents the SEM images of the AT13 coating after wear and the 3-D profilometer image after wear in Fig. 10b. In the SEM images, it is observed that unmelted particles have led to crack propagation toward the substrate, there are some voids and pores between the lamellae, and a weak interfacial structure is present. In the 3-D profilometer image, the porous defects on the surface are noticeable.

In Fig. 11c, the SEM image of the surface of the AT40 sample after the wear test is shown. Figure 11b provides the 3-D profilometer image of AT40 after wear. These images detail the microstructural changes and surface roughness of the coating after wear. Plasma-sprayed coatings exhibit a lamellar-like structure and contain numerous pores and microcracks. These structural defects reduce the density and adhesion strength of the coating. As a result, plasma-sprayed coatings can easily fracture due to the combined effects of high porosity, weak adhesion strength, and low ductility. Additionally, the microcracks in or newly formed within the plasma-sprayed coatings propagate rapidly and eventually connect, leading to further material loss. Therefore, the predominant wear mechanism in plasma-sprayed coatings is the disintegration of the coating [42].

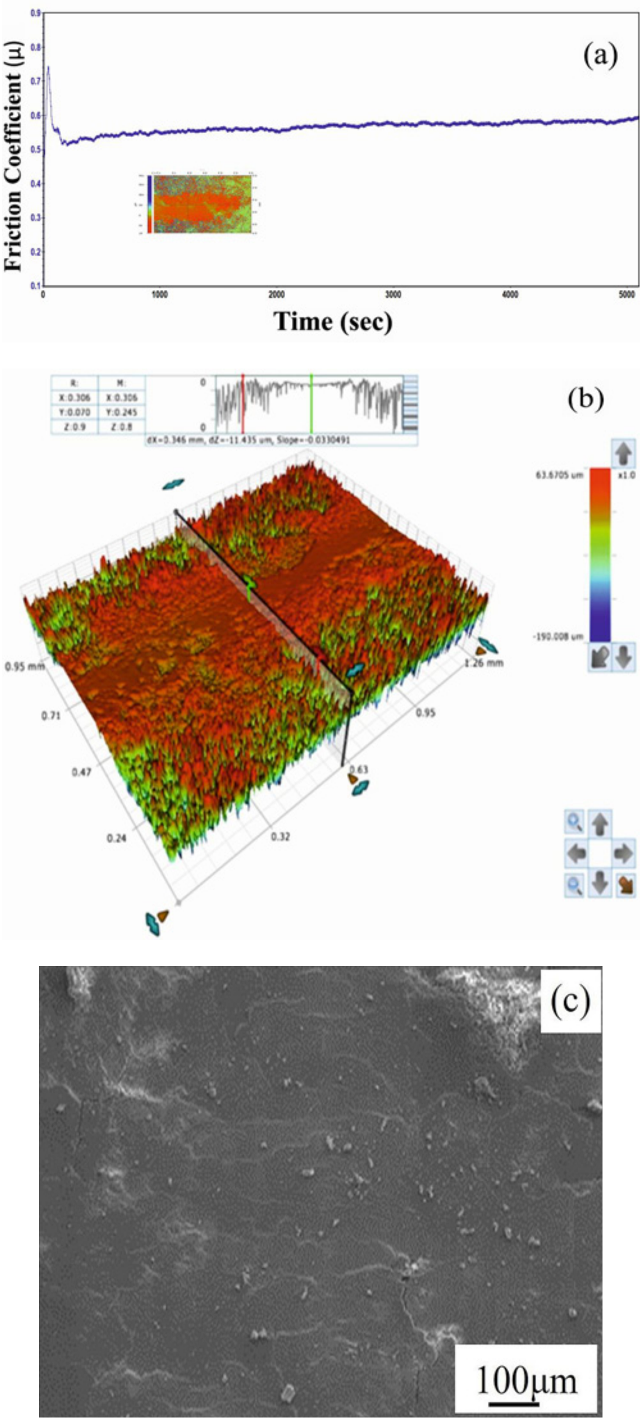

Fig. 11. Wear test results of AT40: (a) friction coefficient-time graph, (b) 3D profilometer image of wear scar, and (c) SEM image of wear scar.

The coatings contain lamellar splashes, small microcracks, and partially melted regions. Due to the high-temperature flame, lamellar cracks have formed on the coating surface. These cracks result from the coating's intense exposure to the high heat generated during the flame spraying process. During the flame process, the powder particles exhibit different behaviors; some particles completely melt, forming a region, while others create partially melted areas. This phenomenon may be attributed to the distribution of the powder particles and the temperature distribution within the flame spray torch [12].

4. Conclusions

In this study, three different surface treatments were applied to AA 5083 aluminum alloy samples using the plasma spraying method. After the surface treatments, the thickness of the resulting films, XRD analyses, surface morphology, scratch tests, and wear tests were conducted. The analysis results were compared with untreated samples. The findings from these analyses are presented below:

– Upon examining the XRD patterns of the coatings obtained through plasma spraying, it was observed that as the TiO_2 content in the coating increased, the intensity of Al_2O_3 peaks decreased.

– Regarding coating thickness, the highest value (512 μm) was found in the AT13 sample.

SEM images revealed a porous structure and the presence of unmelted or partially melted regions in the coatings obtained through plasma spraying.

– The scratch tests indicated that the highest critical load, at 52 N, occurred in the AT0 sample, while the lowest critical load, at 36 N, was observed in the AT13 sample.

– The adhesion of the coatings on the AA 5083 surfaces was generally good; however, during the scratch test of AT13, fluctuations were observed in the sample, possibly due to lower adhesion.

– In the microhardness tests of the coatings, the highest hardness was recorded as $1426 \pm 57\,HV_{0.1}$ in the AT0 sample, while the lowest microhardness was observed in the AT40 coating ($826 \pm 32\ HV_{0.1}$). It was found that the hardness of the coating decreased as the TiO_2 content in the Al_2O_3 coating increased.

– The wear tests demonstrated that all coated samples exhibited better wear resistance than the untreated substrate material. It was also determined that the coefficient of friction increased with the rise in TiO_2 content in the coatings applied via the plasma spraying method.

Acknowledgements

The authors wish to express their gratitude for the technical support provided by Senkron Surface Technologies and Sampa Otomotiv A.S.

References

[1] A. Serkan, G. Behçet, Effect of mechanical properties of AISI 1018 steel surface coating Stellite 6 by GTA method, J. Advanced Technol. Sciences 2 (2013) 62–76.

[2] J. Fahim, H. Ghayour, S. M. M. Hadavi, S. A. H. Tabrizi, Fabrication of superhydrophobic Al5083 aluminum alloy for marine applications, Prot. Met. Phys. Chem. Surfaces 54 (2018) 899–908. https://doi.org/10.1134/S2070205118050052.

[3] B. A. Khan, A. Kumar, P. Suresh, Tribological behaviour of plasma sprayed Al_2O_3-TiO_2 coating on Al-6082T6 substrate, Int. J. Innov. Res. Sci. Eng. Technol. 3 (2014) 13956–13963.

[4] V. P. Muhamed Shajudheen, S. Saravana Kumar, V. Senthil Kumar, A. Uma Maheswari, M. Sivakumar, S. R. Mohan, Study of anticorrosive nature of spray coated titanium dioxide and nickel oxide composite thin films on stainless steel in briny surroundings, AIP Conf. Proc. AIP(2019), pp. 1–9. ISBN 978-073-54190-7-0

[5] M. A. Zavareh, A. A. D. M. Sarhan, R. Karimzadeh, R. Singh, I. K. Singh, Analysis of corrosion protection behavior of Al_2O_3-TiO_2 oxide ceramic coating on carbon steel pipes for petroleum industry, Ceram. Int. 44 (2018) 5967–5975. https://doi.org/10.1016/j.ceramint.2017.12.175.

[6] A. Orłowicz, M. Mróz, M. Tupaj, B. Kupiec, L. Kozak, T. Kij, Application of ceramic coating to improve abrasive wear resistance of die inserts used to press-mould stampings of refractories, Metalurgija 56 (2017) 415–418.

[7] C. Yapıcı, Investigation of AITI5B1 Master Alloy Use as Grain Refiner on Aluminium High Pressure Die Casting Process, İstanbul 2012.

[8] Ç. Çakanyıldırım, M. Gürü, Developments in aluminium production technologies environmental impact and application areas, Journal of Polytechnic 24 (2021) 585–592.(in Turkish) https://doi.org/10.2339/politeknik.707885

[9] M. Ardelean, S. Lascau, E. Ardelean, A. Josan, Surface treatments for aluminium alloys, IOP Conf Ser Mater Sci Eng, ICAS 294 (2018) 012042. https://doi.org/10.1088/1757-899X/294/1/012042.

[10] M. Meikandan, M. Karthick, L. Natrayan, P. P. Patil, S. Sekar,Y. S. Rao, Experimental investigation on tribological behaviour of various processes of anodized coated piston for engine application, J. Nanomater. 2022 (2022) 7983390. https://doi.org/10.1155/2022/7983390

[11] M. Ak, Effect of Impurity Iron on the Mechanical Properties of AA206 Aluminium Casting Alloy, Istanbul, 2012.

[12] D. Kumar, Q. Murtaza, R. S. Walia, P. Singh, Comparative investigation on thermally sprayed Al_2O_3, Al_2O_3-13%(TiO_2) and Al_2O_3-40%(TiO_2) composite coatings from room to 400 °C temperature, Surf. Topogr. Metrol. Prop. 10 (2022) 015043. https://doi.org/10.1088/2051-672X/ac5a75

[13] T. N. Van, T. A. Nguyen, H. P. Thi, L. P. Thi, P. N. Thi, Q. L. Thu, Fabrication and characterization of plasma-sprayed Cr_3C_2-25Cr/Al_2O_3-40TiO_2 duplex coating, J. Therm. Spray Technol. 31 (2022) 2112–2125. https://doi.org/10.1007/s11666-022-01423-y

[14] F. Nafa, H. Bensabra, J. P. Chopart, M. L. Chelagmia, Effect of temperature on anti-corrosion properties of aluminum alloy anodized by sulphuric acid, Rev.

Roum. Chim. 68 (2023) 27–37. https://doi.org/10.33224/rrch.2023.68.1-2.03

[15] M. Michalak, L. Łatka, P. Sokołowski, R. T. Candidato, A. Ambroziak, Effect of TiO_2 on the microstructure and phase composition of Al_2O_3 and Al_2O_3-TiO_2 APS sprayed coatings, Bull. Polish Acad. Sci. Tech. Sci. 69 (2021) 14–17. https://doi.org/10.24425/bpasts.2021.136735

[16] J. Rong, K. Yang, H. Zhao, C. Liu, Y. Zhuang, S. Tao, Tribological performance of plasma sprayed Al_2O_3-Y_2O_3 composite coatings, Surf. Coatings Technol. 302 (2016) 487–494. https://doi.org/10.1016/j.surfcoat.2016.06.053

[17] Z. Yin, S. Tao, X. Zhou, C. Ding, Particle in-flight behavior and its influence on the microstructure and mechanical properties of plasma-sprayed Al_2O_3 coatings, J. Eur. Ceram. Soc. 28 (2008) 1143–1148. https://doi.org/10.1016/j.jeurceramsoc.2007.09.050

[18] P. Fauchais, M. Fukumoto, A. Vardelle, M. Vardelle, Knowledge concerning splat formation: An invited review, J. Therm. Spray Technol. 13 (2004) 337–360. https://doi.org/10.1361/10599630419670.

[19] A. Ganvir, S. Goel, S. Govindarajan, A. R. Jahagirdar, S. Björklund, U. Klement, Tribological performance assessment of Al_2O_3-YSZ composite coatings deposited by hybrid powder-suspension plasma spraying, Surf. Coatings Technol. 409 (2021) 126907. https://doi.org/10.1016/j.surfcoat.2021.126907

[20] R. McPherson, On the formation of thermally sprayed alumina coatings, J. Mater. Sci. 15 (1980) 3141–3149. https://doi.org/10.1007/BF00550387

[21] B. Benli, İ. Çelik, Surface modification and analysis of St37 steel with Al_2O_3-TiO_2, ZrO_2, and Cr_2O_3 ceramic coatings: Structural, mechanical, and tribological properties, Tribol. Int. 191 (2024) 109183. https://doi.org/10.1016/j.triboint.2023.109183

[22] İ. Çelik, Structure and surface properties of Al_2O_3–TiO_2 ceramic coated AZ31 magnesium alloy, Ceram. Int. 42 (2016) 13659–13663. https://doi.org/10.1016/j.ceramint.2016.05.162

[23] J. Iwaszko, Surface remelting treatment of plasma-sprayed Al_2O_3+13wt.% TiO_2 coatings, Surf. Coatings Technol. 201 (2006) 3443–3451. https://doi.org/10.1016/j.surfcoat.2006.07.234

[24] C. Zhang, B. Huang, J. Xu, W. Cao, G. Sun, J. Xiao, Effect of Mo on tribological behaviors of atmospheric plasma sprayed Al_2O_3-13%TiO_2/Mo coatings under boundary lubrication condition, Ceram. Int. 46 (2020) 15066–15075. https://doi.org/10.1016/j.ceramint.2020.03.041

[25] J. J. Zhang, Z. H. Wang, P. H. Lin, L. Q. Si, G. J. Shen, Z. H. Zhou, Corrosion of plasma sprayed NiCrAl/Al_2O_3-13wt.%TiO_2 coatings with and without sealing, Surf. Eng. 28 (2012) 345–350. https://doi.org/10.1179/1743294412Y.0000000004

[26] K. A. Habib, J. J. Saura, C. Ferrer, M. S. Damra, E. Giménez, L. Cabedo, Comparison of flame sprayed Al_2O_3/TiO_2 coatings: Their microstructure, mechanical properties and tribology behavior, Surf. Coatings Technol. 201 (2006) 1436–1443. https://doi.org/10.1016/j.surfcoat.2006.02.011

[27] J. Sure, A. R. Shankar, B. N. Upadhyay, U. K. Mudali, Microstructural characterization of plasma sprayed Al_2O_3-40 wt.%TiO_2 coatings on high density graphite with different post-treatments, Surf. Coatings Technol. 206 (2012) 4741–4749. https://doi.org/10.1016/j.surfcoat.2012.01.058

[28] R. Yılmaz, A. O. Kurt, A. Demir, Z. Tatlı, Effects of TiO_2 on the mechanical properties of the Al_2O_3-TiO_2 plasma sprayed coating, J. Eur. Ceram. Soc. 27 (2007) 1319–1323. https://doi.org/10.1016/j.jeurceramsoc.2006.04.099

[29] Y. Yang, W. Zhou, Z. Tong, L. Chen, X. Yang, E. A. Larson, Electrochemical corrosion behavior of 5083 aluminum alloy subjected to laser shock peening, J. Mater. Eng. Perform. 28 (2019) 6081–6091. https://doi.org/10.1007/s11665-019-04299-2

[30] R. Krishnan, S. Dash, C. B. Rao, R. V. S. Rao, A. K. Tyagi, Laser induced structural and microstructural transformations of plasma sprayed Al_2O_3 coatings, Scr. Mater. 45 (2001) 693–700. https://doi.org/10.1016/S1359-6462(01)01081-8

[31] F. L. Toma, C. C. Stahr, L. M. Berger, S. Saaro, M. Herrmann, D. Deska, G. Michael, Corrosion resistance of APS- and HVOF-sprayed coatings in the Al_2O_3-TiO_2 system, J. Therm. Spray. Technol. 19 (2010) 137–147. https://doi.org/10.1007/s11666-009-9422-2

[32] M. U. Devi, New phase formation in Al_2O_3-based thermal spray coatings, Ceram. Int. 30 (2004) 555–565. https://doi.org/10.1016/j.ceramint.2003.07.002

[33] Ş. Yılmaz, M. Ipek, G. F. Celebi, C. Bindal, The effect of bond coat on mechanical properties of plasma-sprayed Al_2O_3 and Al_2O_3-13 wt.%TiO_2 coatings on AISI 316L stainless steel, Vacuum 77 (2005) 315–321. https://doi.org/10.1016/j.vacuum.2004.11.004

[34] G. Goller, The effect of bond coat on mechanical properties of plasma sprayed bioglass-titanium coatings, Ceram. Int. 30 (2004) 351–355. https://doi.org/10.1016/S0272-8842(03)00107-X

[35] S. Islak, S. Buytoz, E. Ersoz, N. Orhan, J. Stokes, M. S. Hashmi, I. Somunkiran, N. Tosun, Effect on microstructure of TiO_2 rate in Al_2O_3-TiO_2 composite coating produced using plasma spray method, Optoelectron Adv. Mater. Rapid. Commun. 6 (2012) 844–849.

[36] S. Karaoğlu, E. Sonuvar, Structural and wear behavior of coatings formed on AA7075 aluminum alloy by plasma electrolytic oxidation, Pamukkale Univ. Eng. Sci. J. 23 (2017) 405–410. (in Turkish) https://doi.org/10.5505/pajes.2016.24434

[37] P. Bagde, S. G. Sapate, R. K. Khatirkar, N. Vashishtha, Friction and abrasive wear behaviour of Al_2O_3-13TiO_2 and Al_2O_3-13TiO_2+Ni graphite coatings, Tribol. Int. 121 (2018) 353–372. https://doi.org/10.1016/j.triboint.2018.01.067

[38] B. Benli, Surface modification and analysis of St37 steel with different coating methods, Samsun, 2023.

[39] Y. Sert, N. Toplan, Tribological behavior of a plasma-sprayed Al_2O_3-TiO_2-Cr_2O_3 coating, Mater. Technol. 47 (2013) 181–183.

[40] J. A. Wahab, M. J. Ghazali, A. F. S. Baharin, Microstructure and mechanical properties of plasma sprayed Al_2O_3-13%TiO_2 ceramic coating, Matec Web. Conf. 87 (2017) 02027. https://doi.org/10.1051/matecconf/20178702027

[41] L. Łatka, M. Szala, M. Michalak, T. Pałka, Impact of atmospheric plasma spray parameters on cavitation erosion resistance of Al_2O_3-13%TiO_2 coatings, Acta

Phys. Pol. A 136 (2019) 342–347.
https://doi.org/10.12693/APhysPolA.136.342

[42] K. Yang, J. Li, Q. Y. Wang, Z. Li, Y. Jiang, Y. Bao, Effect of laser remelting on microstructure and wear resistance of plasma sprayed Al_2O_3-40%TiO_2 coating, Wear 426–427 (2019) 314–318. https://doi.org/10.1016/j.wear.2019.01.100